Aerospace Science and Technology 32 (2014) 121–130

Contents lists available at ScienceDirect

Aerospace Science and Technology

www.elsevier.com/locate/aescte

# A new dynamic calibration method for IMU deterministic errors of the INS on the Hypersonic Cruise Vehicles

Hui Peng [1], Zhi Xiong [*,2], Rong Wang, Jian-ye Liu, Cheng Zhang

*College of Automation Engineering, Nanjing University of Aeronautics & Astronautics, Nanjing 210016, China*

ARTICLE INFO

*Article history:*
Received 24 January 2013
Received in revised form 12 September 2013
Accepted 6 November 2013
Available online 28 November 2013

*Keywords:*
Hypersonic Cruise Vehicles
Inertial Navigation System
IMU Error modeling
Kalman Filter
Dynamic calibration

ABSTRACT

The Hypersonic Cruise Vehicles (HCVs) have an extremely high requirement for the navigation system to be high-reliable, high-autonomic and high-accurate. This paper proposed a method to calibrate the deterministic errors of the Inertial Measurement Unit (IMU) of the Inertial Navigation System (INS) dynamically. Including the installation errors and the scale factor errors of the IMU, an augmented error model of the IMU and the navigation parameter error propagation equations of INS are discussed first. Then a method based on the Kalman Filter is designed to calibrate deterministic errors of the IMU during the HCV's high dynamic flight process. The proposed method can accurately and dynamically calibrate the deterministic errors of the IMU. The calibration results are used to correct the IMU deterministic errors and the INS parameter errors dynamically. Simulation is made to verify the performance of the calibration method proposed by this paper. The simulation results show that the dynamic calibration method can effectively estimate the installation errors and the scale factor errors of the IMU; the precision of the INS is improved after the compensation of the installation errors and the scale factor errors that obtained by the calibration method.



## 1. Introduction

In recent years, the Hypersonic Cruise Vehicles (HCVs) have already been the research focus in aeronautic and aerospace fields with their great strategic military application values. The high dynamic characteristics of the HCVs have put forward high requirements to the accuracy and reliability of the autonomous navigation systems. The Inertial Navigation System (INS) may be the kernel navigation system of the hypersonic vehicles for the advantages of its high reliability and continuous outputs [8,10].

The measurement errors of the Inertial Measurement Unit (IMU-gyros and accelerometers) are the main factors that affect the precision of the INS. It is generally believed that the installation errors and scale factor errors are fully compensated by the static calibration tests with the turntables and only should the stochastic errors be considered in the IMU error model [13–15,17]. However, during the hypersonic and high dynamic flight process, the installation errors and scale factor errors of IMU may magnify seriously due to the effects of strong vibration, changes in atmospheric conditions, the coupled physical fields influences and the shock interferences [3]. This change may affect the navigation accuracy significantly when the IMU deterministic errors cannot be calibrated and compensated. Hence, it is necessary to build the error model of the IMU deterministic errors.

In recent years, the calibration methods of the IMU deterministic errors are still kept in research. Generally, the multi-position static tests or angular rate tests with turntables are used for the calibration of the IMU deterministic errors [4,7,11]. A linear calibration method is performed by using a turntable to collect data with different angular rates of gyros and utilizing the wavelet signal processing to analyze the data [9]. A dynamic test method with a combination of a single-axis rate-table test and an attitude change mount is used to process the calibrations [6]. The direct IMU calibration method referred in Ref. [5] uses the signals of the previously calibrated IMU to align the IMU that needs calibrating. More than two IMUs are used to process the calibration of the IMU installation errors in Ref. [16]. However, the general turntable and the multi-IMU calibration methods may be no longer applicable due to the space limitation and environmental constraints in the HCV's high dynamic flight process. Hence, based on the Kalman Filter, a method to dynamically calibrate and compensate the installation errors and scale factor errors of the IMU is proposed in this paper. The proposed method could effectively calibrate the deterministic errors of IMU during the dynamic flight process; the calibration results are used to compensate the INS so as to improve the precision of the INS.

* Corresponding author. Tel.: +86 25 84892304 806; fax: +86 25 84892304 819.
*E-mail addresses:* xznuaa@nuaa.edu.cn, xz203@163.com, penghui@nuaa.edu.cn (X. Zhi).
[1] Tel.: +86 25 84892304 854; fax: +86 25 84892304 819.
[2] Zhi Xiong is a professor in College of Automation Engineering, Nanjing University of Aeronautics and Astronautics.

1270-9638/$ – see front matter 
http://dx.doi.org/10.1016/j.ast.2013.11.005

## 2. INS and IMU error modeling

The propagation characteristics of the INS parameter errors are described through the IMU error model and the INS parameter error model. Hence, for studying the influence of the IMU deterministic errors on the navigation performance of INS, it is necessary to build the IMU deterministic error and establish the dynamic error propagation equations of the INS.

### 2.1. General IMU error model

In the general IMU error model, the installation errors and scale factor errors are usually believed fully compensated and the errors of the IMU are supposed to be random drift and zero-offset [15,17]. The general error models of accelerometers and gyros are:

$$\left.\begin{aligned}\delta \boldsymbol{f}^b &= \nabla^b \\ \delta \boldsymbol{\omega}_{ib}^b &= \boldsymbol{\varepsilon}^b\end{aligned}\right\} \tag{1}$$

where $\nabla^b = [\,\nabla_x \quad \nabla_y \quad \nabla_z\,]^T$ are zero-offsets of three accelerometers in the $xyz$ direction of the body frame. All of them are supposed to be the first-order Markov process in the general error models, i.e.:

$$\dot{\nabla} = -\frac{1}{T_a}\nabla + \boldsymbol{w}_a \tag{2}$$

where $T_a$ is the first-order Markov correlation time and $\boldsymbol{w}_a$ is the independent zero-mean Gaussian white-noise processes.

The random drifts of gyros $\boldsymbol{\varepsilon} = [\,\varepsilon_x \quad \varepsilon_y \quad \varepsilon_z\,]^T$ can be described as $\boldsymbol{\varepsilon} = \boldsymbol{\varepsilon}_b + \boldsymbol{\varepsilon}_r + \boldsymbol{w}_g$, where $\boldsymbol{w}_g$ is the independent zero-mean Gaussian white-noise processes, $\boldsymbol{\varepsilon}_b$ is a random constant and $\boldsymbol{\varepsilon}_r$ is the first-order Markov process.

$$\left.\begin{aligned}\dot{\boldsymbol{\varepsilon}}_b &= 0 \\ \dot{\boldsymbol{\varepsilon}}_r &= -\frac{1}{T_g}\boldsymbol{\varepsilon}_r + \boldsymbol{w}_r\end{aligned}\right\} \tag{3}$$

where $T_g$ is the first-order Markov correlation time and $\boldsymbol{w}_r$ is the independent zero-mean Gaussian white-noise processes.

### 2.2. Augmented IMU error model

The accelerometers and gyros are directly mounted on the vehicles during the HCV's high dynamic flight process. Theoretically, the coordinate axis of IMU should be strictly coincident with the body axis of the vehicle. Actually, the HCV's body deformation caused by the strong vibration factors will lead to the non-coincidence between the IMU axis and the body axis. Thus, the installation errors and the scale factor errors may magnify obviously and this phenomenon may lead to the precision of the INS to decrease sharply. Hence, it is essential to model the IMU errors that including the installation errors and the scale factor errors.

- ***Accelerometer error model***

Including the installation errors and the scale factor errors of the accelerometers, the error model of the accelerometer in the augmented IMU error model should be:

$$\delta \boldsymbol{f}^b = [\delta \boldsymbol{K}_A + \delta \boldsymbol{A}]\boldsymbol{f}^b + \nabla^b \tag{4}$$

where $\delta \boldsymbol{K}_A = \mathrm{diag}[\,\delta K_{Ax} \quad \delta K_{Ay} \quad \delta K_{Az}\,]$ is scale factor error matrix of the three accelerometers.

$$\delta \boldsymbol{A} = \begin{bmatrix} 0 & \delta A_z & -\delta A_y \\ -\delta A_z & 0 & \delta A_x \\ \delta A_y & -\delta A_x & 0 \end{bmatrix}$$

is the installation error angle matrix of three accelerometers.

Suppose the installation errors and scale factor errors to be random constants and that the error models of three accelerometers are the same. Then the models of the installation errors and the scale factor errors respectively are:

$$\left.\begin{aligned}\delta \dot{\boldsymbol{K}}_A &= 0 \\ \delta \dot{\boldsymbol{A}} &= 0\end{aligned}\right\} \tag{5}$$

the general IMU error model in Section 2.1 is adopted in the zero-offsets $\nabla^b$.

- ***Gyro error model***

Similarly, the gyro error model is

$$\delta \boldsymbol{\omega}_{ib}^b = [\delta \boldsymbol{K}_G + \delta \boldsymbol{G}]\boldsymbol{\omega}_{ib}^b + \boldsymbol{\varepsilon} \tag{6}$$

where $\delta \boldsymbol{K}_G = \mathrm{diag}[\,\delta K_{Gx} \quad \delta K_{Gy} \quad \delta K_{Gz}\,]$ is the scale factor error matrix of three gyros.

$$\delta \boldsymbol{G} = \begin{bmatrix} 0 & \delta G_z & -\delta G_y \\ -\delta G_z & 0 & \delta G_x \\ \delta G_y & -\delta G_x & 0 \end{bmatrix}$$

is the installation error angle matrix of three gyros.

Suppose the installation errors and scale factor errors to be random constants and that the error models of three gyros are the same. Hence:

$$\left.\begin{aligned}\delta \dot{\boldsymbol{K}}_G &= 0 \\ \delta \dot{\boldsymbol{G}} &= 0\end{aligned}\right\} \tag{7}$$

the general IMU error model in Section 2.1 is adopted in the random drift $\boldsymbol{\varepsilon}$.

### 2.3. INS navigation error model

The navigation error differential equations include three basic navigation parameters errors, namely the mathematical platform error angles, the velocity errors and the position errors. The vector equation of INS errors are described as below.

In this paper, the local East–North-Upward (*ENU*) frame is selected as navigation frame. $\phi_E, \phi_N, \phi_U$ are the platform error angles represented in the local *ENU* frame; $V_E, V_N, V_U$ are the velocities of the vehicle in the East, North and Upward direction; $L, \lambda, h$ represent the latitude, the longitude and the altitude of the vehicle respectively. $R$ is the radius of the earth. The transformation matrix

$$C_b^n = \begin{bmatrix} \cos\gamma\cos\psi + \sin\gamma\sin\theta\sin\psi & \cos\theta\sin\psi & \sin\gamma\cos\psi - \cos\gamma\sin\theta\sin\psi \\ -\cos\gamma\sin\psi + \sin\gamma\sin\theta\cos\psi & \cos\theta\cos\psi & -\sin\gamma\sin\psi - \cos\gamma\sin\theta\cos\psi \\ -\sin\gamma\cos\theta & \sin\theta & \cos\gamma\cos\theta \end{bmatrix}$$

is the coordinate transformation matrix from body frame to navigation frame; where $\gamma, \theta, \psi$ are respectively the roll angle, pitch angle and the yaw angle of the vehicle, and $C_b^n = \{C_{ij}\}$, $i, j = 1, 2, 3$.

- ***Dynamic vector equation of mathematical platform error angles***

The dynamic vector equation of platform error angles can be presented as,

$$\begin{aligned}\dot{\boldsymbol{\phi}} = &-\left(\boldsymbol{\omega}_{ie}^n + \boldsymbol{\omega}_{en}^n\right) \times \boldsymbol{\phi} + \delta \boldsymbol{\omega}_{ie}^n + \delta \boldsymbol{\omega}_{en}^n \\ &- C_b^n(\delta \boldsymbol{K}_G + \delta \boldsymbol{G})\boldsymbol{\omega}_{ib}^b - \boldsymbol{\varepsilon}^n\end{aligned} \tag{8}$$

where $\boldsymbol{\phi} = [\,\phi_E \quad \phi_N \quad \phi_U\,]^T$ and $\phi_E, \phi_N$ and $\phi_U$ represent the platform error angles expressed in the navigation frame. $\boldsymbol{\omega}_{ib}^b$ is

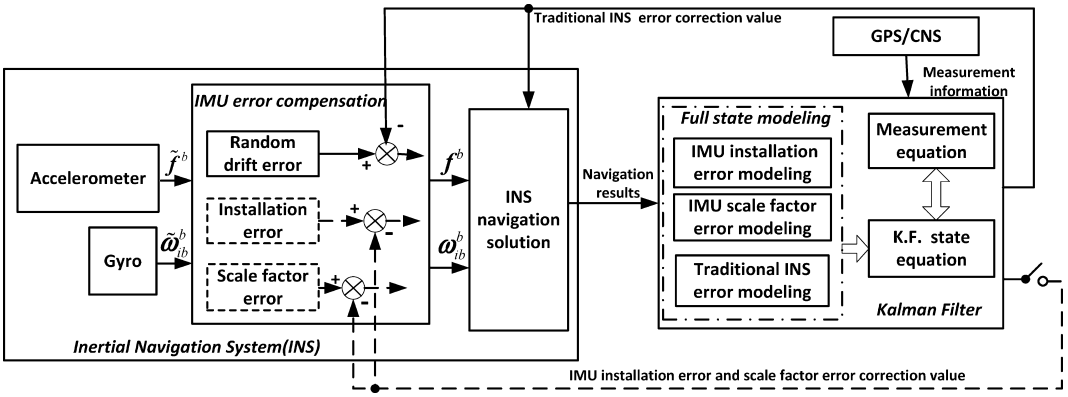


**Fig. 1.** The overall scheme design of the system.

the vehicle body angular rate measured by gyros in the body frame. $\boldsymbol{\omega}_{ie}^{n} = [\,0 \quad \omega_{ie}\cos L \quad \omega_{ie}\sin L\,]^T$ is the projection of the earth rotation rate $\omega_{ie}$ in the navigation frame. $\boldsymbol{\omega}_{en}^{n} = [\,-\frac{V_N}{R+h} \quad \frac{V_E}{R+h} \quad \frac{V_E}{R+h}\tan L\,]^T$ is angular rate of the navigation frame with respect to the earth frame, expressed in the navigation frame.

$$\delta\boldsymbol{\omega}_{ie}^{n} = \begin{bmatrix} 0 \\ -\omega_{ie}\sin L\delta L \\ \omega_{ie}\sin L\delta L \end{bmatrix}$$

and

$$\delta\boldsymbol{\omega}_{en}^{n} = \begin{bmatrix} -\frac{\delta V_N}{R+h} + \delta h\frac{V_N}{(R+h)^2} \\ \frac{\delta V_E}{R+h} - \delta h\frac{V_E}{(R+h)^2} \\ \frac{\delta V_E}{R+h}\tan L + \delta L\frac{V_E\sec^2 L}{R+h} - \delta h\frac{V_E\tan L}{(R+h)^2} \end{bmatrix}$$

are the errors of $\boldsymbol{\omega}_{ie}^{n}$ and $\boldsymbol{\omega}_{en}^{n}$ respectively. $\delta\boldsymbol{K}_G, \delta\boldsymbol{G}$ and $\boldsymbol{\varepsilon}^n$ are defined as that in Sections 2.1 and 2.2.

Including the installation errors and the scale factor errors of the IMU, the part $C_b^n(\delta\boldsymbol{K}_G + \delta\boldsymbol{G})\boldsymbol{\omega}_{ib}^{b}$ is added to the dynamic equations of platform error angles in this paper, which is different from the general INS [13,17] parameter error equations.

- ***Dynamic vector equation of velocity errors***

$$\begin{aligned}\delta\dot{\boldsymbol{V}}^n = &-\boldsymbol{\phi}^n \times \boldsymbol{f}^n + C_b^n(\delta\boldsymbol{K}_A + \delta\boldsymbol{A})\boldsymbol{f}^b + \delta\boldsymbol{V}^n \times \left(2\boldsymbol{\omega}_{ie}^{n} + \boldsymbol{\omega}_{en}^{n}\right) \\ &+ \boldsymbol{V}^n \times \left(2\delta\boldsymbol{\omega}_{ie}^{n} + \delta\boldsymbol{\omega}_{en}^{n}\right) + \nabla^n \end{aligned} \tag{9}$$

where $\delta\boldsymbol{V} = [\,\delta V_E \quad \delta V_N \quad \delta V_U\,]^T$ and $\delta V_E, \delta V_N, \delta V_U$ respectively represent the velocity errors in the *ENU* navigation frame. $\boldsymbol{f}^b = [\,f_x^b \quad f_y^b \quad f_z^b\,]^T$ represents the specific force measured by the three accelerometers in the body frame $\boldsymbol{b}$. $\delta\boldsymbol{K}_A, \delta\boldsymbol{A}$ and $\nabla^n$ are defined as that in Sections 2.1 and 2.2. Similar to the platform error angle equations, the added part is $C_b^n(\delta\boldsymbol{K}_A + \delta\boldsymbol{A})\boldsymbol{f}^b$.

- ***Dynamic equation of position errors***

$$\begin{aligned}\delta\dot{L} &= \frac{\delta V_N}{R+h} - \delta h\frac{V_N}{(R+h)^2} \\ \delta\dot{\lambda} &= \frac{\delta V_E}{R+h}\sec L + \delta L\frac{V_E}{R+h}\tan L\sec L - \delta h\frac{V_E\sec L}{(R+h)^2} \\ \delta\dot{h} &= \delta V_U \end{aligned} \tag{10}$$

The instability of the altitude can be restrained through the altitude damping algorithm, so the influence of the altitude channel error $\delta h$ is ignored in the analysis of this paper.

## 3. Dynamic calibration of IMU deterministic errors

Different from the conventional IMU deterministic error calibration methods, this paper proposed a method based on the Kalman Filter to calibrate the installation errors and scale factor errors of the IMU during the HCV's high dynamic flight process. The calibration results are used to compensate the IMU deterministic errors so as to improve the precision of the INS and satisfy the accurately strike requirement of the vehicles.

### 3.1. Scheme design

The system scheme design is shown as Fig. 1.

In Fig. 1, $\tilde{\boldsymbol{f}}^b$ and $\tilde{\boldsymbol{\omega}}_{ib}^{b}$ are respectively the specific force measured by accelerometers and angular rates measured by gyros, both of which contain the deterministic errors and the stochastic errors. The deterministic errors and the stochastic errors of IMU are compensated to get the theoretical values $\boldsymbol{f}^b$ and $\boldsymbol{\omega}_{ib}^{b}$ which are used in the INS navigation solution stage.

In order to compose the improved full state model of the Kalman Filter for the calibration of the IMU deterministic errors, an augmented IMU error model that including the deterministic errors is built and the INS parameter error propagation equations are derived. The Global Position System or the satellite navigation receiver is used to provide the measurement information of position and velocity; the Celestial Navigation System or the star sensor is used to provide the measurement information of attitude of the vehicle during the calibration process.

The calibrated results of the IMU deterministic errors are used to compensate the installation errors and the scale factor errors of the IMU. In order to improve the computational efficiency, when the calibration of the deterministic errors of IMU are finished, the full state Kalman Filter could turn to the traditional one [12,13,15, 18,19] whose state variables don't include the installation errors and scale factor errors of the IMU.

### 3.2. System equations for calibration

In this paper, the *X-Y-Z* direction of the body frame is coincident with the Right-Front-Upward direction of the vehicle body; the local East–North-Upward (*ENU*) frame is selected as navigation frame. The system equations are described as Eq. (11)

$$\left.\begin{aligned}\dot{\boldsymbol{X}}(t) &= \boldsymbol{F}(t)\boldsymbol{X}(t) + \boldsymbol{G}(t)\boldsymbol{W}(t) \\ \boldsymbol{Z}(t) &= \boldsymbol{H}(t)\boldsymbol{X}(t) + \boldsymbol{V}(t)\end{aligned}\right\} \tag{11}$$

where $\boldsymbol{X}(t)$ is the state variables vector, $\boldsymbol{F}(t)$ is the system matrix, $\boldsymbol{G}(t)$ is the error coefficient matrix, $\boldsymbol{W}(t)$ is the system noise matrix, $\boldsymbol{Z}(t)$ is the measurement information matrix, $\boldsymbol{H}(t)$ is the

matrix that reflects the relations between $\boldsymbol{X}(t)$ and $\boldsymbol{Z}(t)$, $\boldsymbol{V}(t)$ is the noise vector of the measurement information.

**1) Kalman Filter state model**

- ***Traditional Kalman Filter state model***

The traditional Kalman Filter state model consists of the basic navigation parameter errors, i.e. three mathematical platform error angles, three velocity errors and the position errors, nine variables in all as the state variables.

In some references, the stochastic errors of the IMU are included in the general Kalman Filter state model as the extended states. The gyro random drifts $(\varepsilon_x, \varepsilon_y, \varepsilon_z)$ and the accelerometer zero-offsets $(\nabla_x, \nabla_y)$ are added to the state variables in Refs. [15] and [19]. The zero-offset error of the accelerometer in the up direction is also added to the state variables in Refs. [14] and [17]. The gyro drifts $(\varepsilon_{bx}, \varepsilon_{by}, \varepsilon_{bz}, \varepsilon_{rx}, \varepsilon_{ry}, \varepsilon_{rz})$ and the accelerometer zero-offsets $(\nabla_x, \nabla_y, \nabla_z)$ are included in the filter state variables, i.e., 18 states in all to construct the Kalman Filter state model in Ref. [13], i.e.

$$\begin{aligned}\boldsymbol{X} = [\,&\phi_E \quad \phi_N \quad \phi_U \quad \delta V_E \quad \delta V_N \quad \delta V_U \quad \delta L \quad \delta\lambda \quad \delta h \\ &\varepsilon_{bx} \quad \varepsilon_{by} \quad \varepsilon_{bz} \quad \varepsilon_{rx} \quad \varepsilon_{ry} \quad \varepsilon_{rz} \quad \nabla_x \quad \nabla_y \quad \nabla_z\,]^T\end{aligned} \tag{12}$$

The corresponding system matrix of the traditional filter state model shown in Eq. (12) is:

$$\boldsymbol{F}(t) = \begin{bmatrix} \boldsymbol{FN}(t)_{9\times 9} & \boldsymbol{FS}(t)_{9\times 9} \\ \boldsymbol{0}_{9\times 9} & \boldsymbol{FM}(t)_{9\times 9} \end{bmatrix} \tag{13}$$

where $\boldsymbol{FN}(t)_{9\times 9}$ is the typical $9\times 9$ matrix that represents the relationships of the basic navigation parameter errors, the non-zero elements of the $\boldsymbol{FN}(t)_{9\times 9}$ are as follows [15]:

$$FN(1,2) = \omega_{ie}\sin L + \frac{V_E}{R+h}\tan L$$
$$FN(1,3) = -\left(\omega_{ie}\cos L + \frac{V_E}{R+h}\right)$$
$$FN(1,5) = -\frac{1}{R+h}$$
$$FN(2,1) = -\left(\omega_{ie}\sin L + \frac{V_E}{R+h}\tan L\right)$$
$$FN(2,3) = -\frac{V_N}{R+h}$$
$$FN(2,4) = -\frac{1}{R+h}$$
$$FN(2,7) = -\omega_{ie}\sin L$$
$$FN(3,1) = \omega_{ie}\cos L + \frac{V_E}{R+h}$$
$$FN(3,2) = \frac{V_N}{R+h}$$
$$FN(3,4) = \frac{\tan L}{R+h}$$
$$FN(3,7) = \omega_{ie}\cos L + \frac{V_E}{R+h}\sec^2 L$$
$$FN(4,2) = -f_u$$
$$FN(4,3) = f_n$$
$$FN(4,4) = \frac{V_N\tan L - V_U}{R+h}$$
$$FN(4,5) = 2\omega_{ie}\sin L + \frac{V_E}{R+h}\tan L$$
$$FN(4,6) = -\left(2\omega_{ie}\cos L + \frac{V_E}{R+h}\right)$$
$$FN(4,7) = 2\omega_{ie}(V_U\sin L + V_N\cos L) + \frac{V_E V_N}{R+h}\sec^2 L$$
$$FN(5,1) = f_u$$
$$FN(5,3) = -f_e$$
$$FN(5,4) = -2\left(\omega_{ie}\sin L + \frac{V_E}{R+h}\tan L\right)$$
$$FN(5,5) = -\frac{V_U}{R+h}$$
$$FN(5,6) = -\frac{V_N}{R+h}$$
$$FN(5,7) = -\left(2V_E\omega_{ie}\cos L + \frac{V_E^2}{R+h}\sec^2 L\right)$$
$$FN(6,1) = -f_n$$
$$FN(6,2) = f_e$$
$$FN(6,4) = 2\left(\omega_{ie}\cos L + \frac{V_E}{R+h}\right)$$
$$FN(6,5) = \frac{2V_N}{R+h}$$
$$FN(6,7) = -2V_E\omega_{ie}\sin L$$
$$FN(7,5) = \frac{1}{R+h}$$
$$FN(8,4) = \frac{\sec L}{R+h}$$
$$FN(8,7) = \frac{V_E}{R+h}\sec L\tan L$$
$$FN(9,6) = 1$$

where $f_n$, $f_e$, $f_u$ are respectively the specific output of the accelerometers in the north, east and the up direction. $\omega_{ie}$ is the earth rotation rate. $\boldsymbol{FS}(t)_{9\times 9}$ is the matrix between the nine navigation parameter errors and the stochastic errors of IMU and

$$\boldsymbol{FS}(t) = \begin{bmatrix} C_b^n & C_b^n & 0_{3\times 3} \\ 0_{3\times 3} & 0_{3\times 3} & C_b^n \\ 0_{3\times 9} & & \end{bmatrix} \cdot \boldsymbol{FM}(t)_{9\times 9}$$

is the matrix that represents the relationships of the IMU stochastic errors and $\boldsymbol{FM}(t) = \mathrm{Diag}[0\ \ 0\ \ 0\ \ -\frac{1}{T_{gx}}\ \ -\frac{1}{T_{gy}}\ \ -\frac{1}{T_{gz}}\ \ -\frac{1}{T_{ax}}\ \ -\frac{1}{T_{ay}}\ \ -\frac{1}{T_{az}}]$.

- ***Improved Kalman Filter state model***

Based on the error modeling of the accelerometers and gyros, the installation errors and the scale factor errors of the IMU are added to the state model of the Kalman Filter so as to construct the improved state model, i.e.

$$\begin{aligned}\boldsymbol{X} = [\,&\phi_E \quad \phi_N \quad \phi_U \quad \delta V_E \quad \delta V_N \quad \delta V_U \quad \delta L \quad \delta\lambda \quad \delta h \quad \varepsilon_{bx} \quad \varepsilon_{by} \\ &\varepsilon_{bz} \quad \varepsilon_{rx} \quad \varepsilon_{ry} \quad \varepsilon_{rz} \quad \nabla_x \quad \nabla_y \quad \nabla_z \quad \delta A_x \quad \delta A_y \quad \delta A_z \quad \delta K_{Ax} \\ &\delta K_{Ay} \quad \delta K_{Az} \quad \delta G_x \quad \delta G_y \quad \delta G_z \quad \delta K_{Gx} \quad \delta K_{Gy} \quad \delta K_{Gz}\,]^T\end{aligned} \tag{14}$$

From the IMU error model built in Section 2.2 (Eqs. (4)–(7)) and the INS errors propagation equations described in Section 2.3 (Eqs. (8)–(10)) the system matrix $\boldsymbol{F}(t)$ of the improved Kalman Filter model is

$$\boldsymbol{F}(t)=\begin{bmatrix}\boldsymbol{FN}(t)_{9\times9} & \boldsymbol{FS}(t)_{9\times9} & \boldsymbol{Fs}(t)_{9\times12}\\ \boldsymbol{0}_{9\times9} & \boldsymbol{FM}(t)_{9\times9} & \boldsymbol{0}_{9\times12}\\ & \boldsymbol{0}_{12\times30} &\end{bmatrix} \tag{15}$$

$\boldsymbol{FN}(t)_{9\times9}$, $\boldsymbol{FS}(t)_{9\times9}$ and $\boldsymbol{FM}(t)_{9\times9}$ is the same as the counterpart of the traditional filter state model and

$$\boldsymbol{Fs}(t)=\begin{bmatrix}\boldsymbol{0}_{3\times6} & \boldsymbol{F}_1(t) & \boldsymbol{F}_3(t)\\ \boldsymbol{F}_2(t) & \boldsymbol{F}_4(t) & \boldsymbol{0}_{3\times6}\\ & \boldsymbol{0}_{3\times12} &\end{bmatrix} \tag{16}$$

where

$$\boldsymbol{F}_1(t)=\begin{bmatrix}-C_{12}\omega^b_{ibz}+C_{13}\omega^b_{iby} & C_{11}\omega^b_{ibz}-C_{13}\omega^b_{ibx} & -C_{11}\omega^b_{iby}+C_{12}\omega^b_{ibx}\\ -C_{22}\omega^b_{ibz}+C_{23}\omega^b_{iby} & C_{21}\omega^b_{ibz}-C_{23}\omega^b_{ibx} & -C_{21}\omega^b_{iby}+C_{22}\omega^b_{ibx}\\ -C_{32}\omega^b_{ibz}+C_{33}\omega^b_{iby} & C_{31}\omega^b_{ibz}-C_{33}\omega^b_{ibx} & -C_{31}\omega^b_{iby}+C_{32}\omega^b_{ibx}\end{bmatrix}$$

$$\boldsymbol{F}_2(t)=\begin{bmatrix}C_{12}f^b_z-C_{13}f^b_y & -C_{11}f^b_z+C_{13}f^b_x & C_{11}f^b_y-C_{12}f^b_x\\ C_{22}f^b_z-C_{23}f^b_y & -C_{21}f^b_z+C_{23}f^b_x & C_{21}f^b_y-C_{22}f^b_x\\ C_{32}f^b_z-C_{33}f^b_y & -C_{31}f^b_z+C_{33}f^b_x & C_{31}f^b_y-C_{32}f^b_x\end{bmatrix}$$

$$\boldsymbol{F}_3(t)=\begin{bmatrix}-C_{11}\omega^b_{ibx} & -C_{12}\omega^b_{iby} & -C_{13}\omega^b_{ibz}\\ -C_{21}\omega^b_{ibx} & -C_{22}\omega^b_{iby} & -C_{23}\omega^b_{ibz}\\ -C_{31}\omega^b_{ibx} & -C_{32}\omega^b_{iby} & -C_{33}\omega^b_{ibz}\end{bmatrix}$$

$$\boldsymbol{F}_4(t)=\begin{bmatrix}C_{11}f^b_x & C_{12}f^b_y & C_{13}f^b_z\\ C_{21}f^b_x & C_{22}f^b_y & C_{23}f^b_z\\ C_{31}f^b_x & C_{32}f^b_y & C_{33}f^b_z\end{bmatrix}$$

where $C_{ij}, i, j = 1, 2, 3$, are the elements of the coordinate transformation matrix $C^n_b$. $\boldsymbol{f}^b = [\,f^b_x \quad f^b_y \quad f^b_z\,]^T$ represents the specific force measured by the three accelerometers in the body frame and $\boldsymbol{\omega}^b_{ib} = [\,\omega^b_{ibx} \quad \omega^b_{iby} \quad \omega^b_{ibz}\,]^T$ is body angular rate measured by three gyros in the body frame. The system noise matrix is $\boldsymbol{W}(t) = [\,w_{gx} \quad w_{gy} \quad w_{gz} \quad w_{rx} \quad w_{ry} \quad w_{rz} \quad w_{ax} \quad w_{ay} \quad w_{az}\,]^T$ and $w_{gx}, w_{gy}, w_{gz}, w_{rx}, w_{ry}, w_{rz}, w_{ax}, w_{ay}, w_{az}$ are the independent zero-mean Gaussian white-noise processes. The state error coefficient matrix is

$$\boldsymbol{G}(t)=\begin{bmatrix}C^n_b & 0_{3\times3} & 0_{3\times3}\\ 0_{9\times3} & 0_{9\times3} & 0_{9\times3}\\ 0_{3\times3} & I_{3\times3} & 0_{3\times3}\\ 0_{3\times3} & 0_{3\times3} & I_{3\times3}\end{bmatrix}$$

**2) Filter measurement model**

As is shown in Section 2.3, the gyro errors and the accelerometer errors are respectively included in the mathematical platform error angle equations and the velocity error equations. Hence, the gyro errors could be estimated through the attitude measurement and the accelerometer errors could be estimated through the velocity measurement. The position measurement could restrain the diffusion of the altitude channel effectively. Hence, the measurement information of attitude, velocity and position of the vehicle are utilized. The system measurement equation is

$$\begin{aligned}\boldsymbol{Z}(t)&=\begin{bmatrix}\boldsymbol{Z}_{\boldsymbol{p}}(t)\\ \boldsymbol{Z}_{\boldsymbol{v}}(t)\\ \boldsymbol{Z}_{\phi}(t)\end{bmatrix}=\begin{bmatrix}\boldsymbol{H}_{\boldsymbol{p}}(t)\\ \boldsymbol{H}_{\boldsymbol{v}}(t)\\ \boldsymbol{H}_{\phi}(t)\end{bmatrix}\boldsymbol{X}(t)+\begin{pmatrix}\boldsymbol{V}_{\boldsymbol{p}}(t)\\ \boldsymbol{V}_{\boldsymbol{v}}(t)\\ \boldsymbol{V}_{\phi}(t)\end{pmatrix}\\ &=\begin{bmatrix}0_{3\times6} & \mathrm{diag}[\,R_M \quad R_N\cos L \quad 1\,] & 0_{3\times21}\\ 0_{3\times3} & \mathrm{diag}[\,1 \quad 1 \quad 1\,] & 0_{3\times24}\\ & \boldsymbol{H}_{\alpha} \quad 0_{3\times27} &\end{bmatrix}\boldsymbol{X}(t)\end{aligned} \tag{17}$$

where $\boldsymbol{Z}_{\boldsymbol{p}}(t), \boldsymbol{Z}_{v}(t)$ and $\boldsymbol{Z}_{\phi}(t)$ are respectively the position measurement information vector, the velocity measurement information vector and the attitude measurement information vector. $\boldsymbol{H}_{\boldsymbol{p}}(t)$, $\boldsymbol{H}_{v}(t)$ and $\boldsymbol{H}_{\phi}(t)$ are the corresponding measurement matrices. $\boldsymbol{V}_{\boldsymbol{p}}(t)$, $\boldsymbol{V}_{\boldsymbol{v}}(t)$ and $\boldsymbol{V}_{\phi}(t)$ are the corresponding noise vectors. $\boldsymbol{H}_{\alpha}(t)$ is the transformation matrix from INS mathematic platform error angles to attitude error angles of the vehicle and

$$\boldsymbol{H}_{\alpha}=\frac{-1}{\cos\theta}\begin{bmatrix}\sin\psi & \cos\psi & 0\\ \cos\psi\cos\theta & -\sin\psi\cos\theta & 0\\ \sin\psi\sin\theta & \cos\psi\sin\theta & -\cos\theta\end{bmatrix}$$

where $\theta$ and $\psi$ are respectively the pitch angle and the yaw angle of the vehicle. $R_M$ and $R_N$ are respectively the curvature radius of the reference ellipsoid in longitude and latitude circles of the earth.

The GPS or the satellite navigation receiver is used to provide the position and velocity measurement information; the CNS or the star sensor is used to provide the attitude measurement information for the calibration. Based on the improved Kalman Filter state model and the measurement equations established, the Kalman Filter is discretized to update the state equations and the measurement equations so as to get the accurate estimate of the deterministic errors of IMU which would be utilized in the error compensation stage.

### 3.3. IMU error compensation algorithm

In the HCV's dynamic flight process, the improved Kalman Filter model built in Section 3.2 is used to get the real-time estimation values of installation errors, scale factor errors of the IMU.

The measurement outputs of the accelerometers and gyros are respectively $\tilde{\boldsymbol{f}}^b$ and $\tilde{\boldsymbol{\omega}}^b_{ib}$, both $\tilde{\boldsymbol{f}}^b$ and $\tilde{\boldsymbol{\omega}}^b_{ib}$ contain the installation errors, the scale factor errors and the stochastic errors, while the ideal theoretical values are respectively $\boldsymbol{f}^b$ and $\boldsymbol{\omega}^b_{ib}$, then

$$\left.\begin{aligned}\tilde{\boldsymbol{f}}^b&=[\boldsymbol{I}+\delta\boldsymbol{K}_A+\delta\boldsymbol{A}]\boldsymbol{f}^b+\nabla^b\\ \tilde{\boldsymbol{\omega}}^b_{ib}&=[\boldsymbol{I}+\delta\boldsymbol{K}_G+\delta\boldsymbol{G}]\boldsymbol{\omega}^b_{ib}+\boldsymbol{\varepsilon}^b\end{aligned}\right\} \tag{18}$$

The compensation algorithm for the IMU errors is

$$\left.\begin{aligned}\boldsymbol{f}^b&=[\boldsymbol{I}-\delta\boldsymbol{K}_A-\delta\boldsymbol{A}]\big(\tilde{\boldsymbol{f}}^b-\nabla^b\big)\\ \boldsymbol{\omega}^b_{ib}&=[\boldsymbol{I}-\delta\boldsymbol{K}_G-\delta\boldsymbol{G}]\big(\tilde{\boldsymbol{\omega}}^b_{ib}-\boldsymbol{\varepsilon}^b\big)\end{aligned}\right\} \tag{19}$$

where $\delta\boldsymbol{K}_A, \delta\boldsymbol{A}, \delta\boldsymbol{K}_G, \delta\boldsymbol{G}$ are the accelerometers and gyros errors that are obtained through the dynamic calibration process.

## 4. Simulation and analysis

In order to verify the performance of the dynamic calibration method proposed in this paper, two groups of calibration simulation results of the IMU deterministic errors are provided. Contrasts between the calibration results and the set values of the installation errors and the scale factor errors have been made.

The parameters of the deterministic and stochastic errors of the IMU and the measurement information noise parameters in the simulation are set as Table 1 and Table 2.

Based primarily on reconstructed trajectory of the X-43A hypersonic research vehicle [1,2], a hypersonic trajectory is designed.

**Table 1**
IMU error parameters.

| Error type | Error parameters | | | Error values |
|---|---|---|---|---|
| Deterministic errors | Group 1 | Gyros | Installation errors ($\delta \boldsymbol{G}$) | $10''$ |
| | | | Scale factor errors ($\delta \boldsymbol{K}_G$) | 100 ppm |
| | | Accelerometer | Installation errors ($\delta \boldsymbol{A}$) | $600''$ |
| | | | Scale factor errors ($\delta \boldsymbol{K}_A$) | 1500 ppm |
| | Group 2 | Gyros | Installation errors ($\delta \boldsymbol{G}$) | $20''$ |
| | | | Scale factor errors ($\delta \boldsymbol{K}_G$) | 50 ppm |
| | | Accelerometers | Installation errors ($\delta \boldsymbol{A}$) | $200''$ |
| | | | Scale factor errors ($\delta \boldsymbol{K}_A$) | 500 ppm |
| Stochastic errors | Gyros | Random constant errors ($\boldsymbol{\varepsilon}_b$) | | $0.01^\circ$/h |
| | | First-order Markov process ($\boldsymbol{\varepsilon}_r$) | | correlation time is 3600 s, variance of white-noise is $0.01^\circ$/h |
| | Accelerometers | First-order Markov process ($\nabla$) | | correlation time is 1800 s, variance of white-noise is $10^{-4}$ g |

**Table 2**
Measurement information noise parameters.

| Parameters | Attitude precision (units: deg) | | | Velocity precision (units: m/s) | | | Position precision (units: m) | | |
|---|---|---|---|---|---|---|---|---|---|
| | Roll | Pitch | Yaw | East | North | Up | Longitude | Latitude | Altitude |
| Values | 0.01 | 0.01 | 0.01 | 0.1 | 0.1 | 0.1 | 5 | 5 | 10 |

**Table 3**
Maneuvers of the hypersonic vehicle.

| Time | Flight phase | Angular rate (units: deg/s) | | | Axial acceleration (units: G) | Velocity |
|---|---|---|---|---|---|---|
| | | Roll rate | Pitch rate | Yaw rate | | |
| 0–4 s | Acceleration and climbing | 0 | 0 | 0 | 7.0 | Accelerating form 300 m/s to Mach 6.1 |
| 4–6 s | | 0 | 15 | 0 | 7.0 | |
| 6–24 s | | 0 | 0 | 0 | 7.0 | |
| 24–26 s | | 0 | −15 | 0 | 7.0 | |
| 26–28 s | Attitude adjusting | 90 | 0 | 0 | 0 | |
| 28–30 s | Separation | −90 | 0 | 0 | 2.0 | |
| 30–35 s | Scramjet engine working and calibration | 0 | 0 | 2 | 2.0 | From Mach 6.1 to Mach 10 |
| 35–40 s | of IMU deterministic errors | 2 | 0 | −2 | 2.0 | |
| 40–45 s | | 0 | 2 | 0 | 2.0 | |
| 45–50 s | | −2 | −2 | 0 | 2.0 | |
| 50–200 s | | 0 | 0 | 0 | 2.0 | |
| 200–900 s | Cruise flight | 0 | 0 | 0 | 0 | Mach 10 |
| 900–950 s | Descent | 0 | −0.2 | 0 | 0 | – |

The initial position of the vehicle is 118 °E, 60 °N. The output frequency of the INS is 100 Hz, the filtering cycle is 1 s. The angular rate and the acceleration information are designed as Table 3.

The designed trajectory of the hypersonic vehicle started from the moment that the vehicle was dropped from the carrier airplane and the rocket booster began to work. The HCV started to climb and accelerate under the propelling of the rocket booster. It was accelerated to Mach 6.1 in about 26 s powered by the rocket booster [2]. When the rocket booster burnt out, the vehicle adjusted its attitude and then the booster was separated from the HCV. After the separation of the booster, the scramjet engine lit and the vehicle was accelerated to Mach 10 at approximately 24,000 m. The vehicle cruised for about 700 s and then splashed down; the descent lasted for 50 s in our designed trajectory.

The designed trajectory and the velocity of the hypersonic vehicle is shown in Fig. 2.

In our designed trajectory, when the vehicle was dropped from the carrier airplane, the velocity was about 300 m/s. The velocity of the vehicle approximately reached to Mach 6.1 when the end of the acceleration and climbing stage. The scramjet engine began to work and then the calibration stage began; the velocity was about Mach 6.1 during the calibration stage. The vehicle was accelerated by the scramjet engine to about Mach 10, and then the vehicle began to cruise. In the calibration stage, the HCV was designed to do some small maneuvers and the calibration lasted for about 150 s. The calibration results of the IMU deterministic errors are simulated below.

**1) Calibration simulation**

The proposed calibration method is verified by the simulation and the results are shown in Fig. 3 and Fig. 4. Fig. 3 is the calibration results of the first group of the IMU deterministic errors and Fig. 4 is the calibration results of the second group of the IMU deterministic errors in Table 1. In both Fig. 3 and Fig. 4, the red dash dot lines represent the set values of the installation errors and the scale factor errors; the black solid lines represent the calibration results. In order to make sure the calibration results more accurate and stable, the abscissas of Figs. 3 and 4 are from 0 s to 200 s. The start of the abscissa 0 s corresponds with the start time of the calibration process, and it is also the start of the 4th flight stage in Table 3. The labeled longitudinal axis ($x$, $y$ and $z$ axis) in each figure represents the measurement output errors of the three gyros or accelerometers in three directions.

The estimation errors of the calibration results are assumed to be $\delta x = \hat{x} - x$, where $\hat{x}$ and $x$ respectively represent the calibration results and the true values of the IMU installation errors and the scale factor errors; the Root Mean Square (RMS) of $\delta x$ is defined as

$$RMS(\delta x) = \sqrt{E\left(\delta x^2\right)} \cong \sqrt{\frac{1}{N}\sum_{i=1}^{N}(\delta x_i)^2} \tag{20}$$

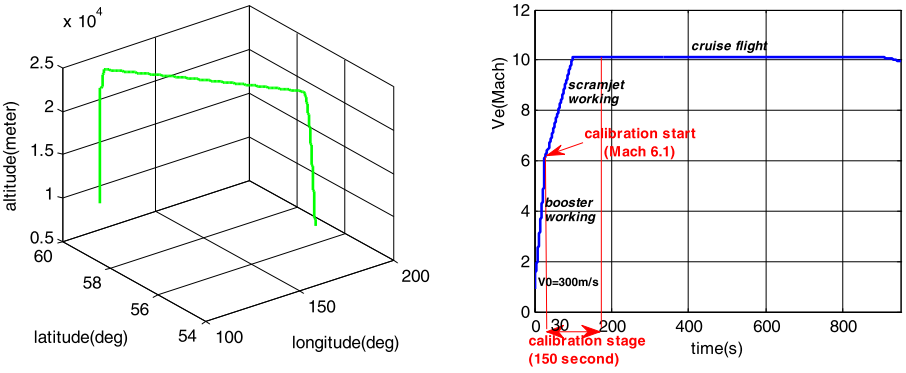


a) Trajectory of the hypersonic vehicle b) the velocity of each flight stage

**Fig. 2.** Trajectory and the velocity of the hypersonic vehicle.

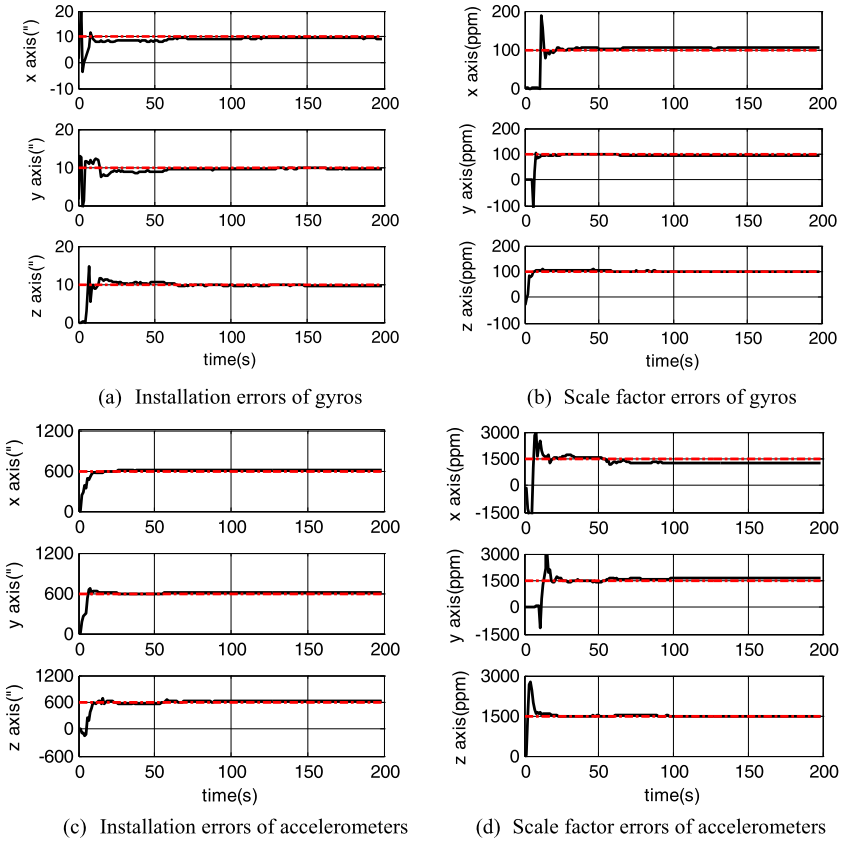


(a) Installation errors of gyros (b) Scale factor errors of gyros

(c) Installation errors of accelerometers (d) Scale factor errors of accelerometers

**Fig. 3.** Calibration results of the first group of the IMU deterministic errors.

**Table 4**
RMS results for the estimation errors of the calibration results.

| Error type | Accelerometers | | | | | | Gyros | | | | | |
|---|---|---|---|---|---|---|---|---|---|---|---|---|
| | Installation errors (units: arc second) | | | Scale factor errors (units: ppm) | | | Installation errors (units: arc second) | | | Scale factor errors (units: ppm) | | |
| Axis | *x* | *y* | *z* | *x* | *y* | *z* | *x* | *y* | *z* | *x* | *y* | *z* |
| Group 1 | 15.9 | 7.97 | 3.75 | 55.7 | 78.2 | 47.9 | 0.25 | 0.52 | 1.43 | 7.75 | 9.86 | 2.46 |
| Group 2 | 1.09 | 3.44 | 5.01 | 27.1 | 40.3 | 11.9 | 0.30 | 0.58 | 0.33 | 8.97 | 9.02 | 3.14 |

The statistical data begins form the 100th second when the calibration results are stable to the 200th second. Table 4 shows the RMS results for the calibration errors.

From the simulation curves shown in Fig. 3, Fig. 4 and Table 4, we can see that the estimated values of the installation errors and scale factor errors tend to be stable after 100 s. The proposed calibration method can effectively calibrate the deterministic errors of the IMU.

**2) Compensation simulation**

With the first group of the deterministic errors set in Table 1 and the corresponding calibration results, the contrast results of the compensated and uncompensated INS parameter errors are simulated below. The compensation is started after the calibration of the IMU deterministic errors. The start time of the compensation simulation was at the 200th second when the calibration of the IMU deterministic errors are finished, and it is also the time

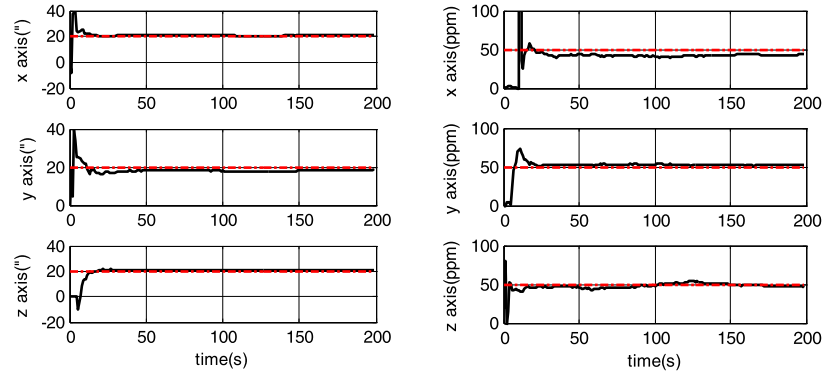


(a) Installation errors of gyros (b) Scale factor errors of gyros

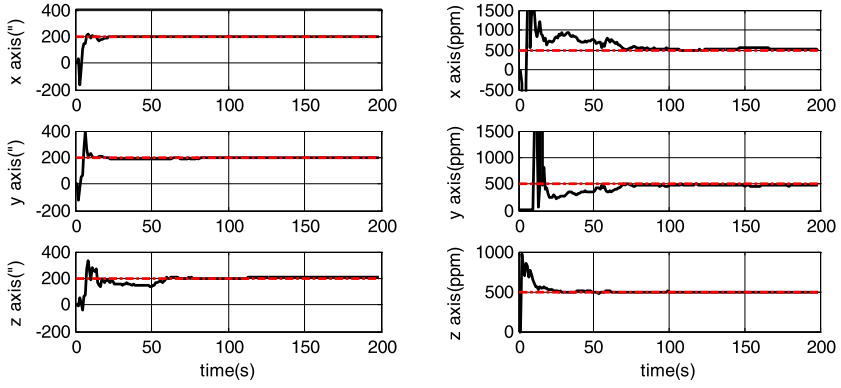


(c) Installation errors of accelerometers (d) Scale factor errors of accelerometers

**Fig. 4.** Calibration result of the second group of the IMU deterministic errors.

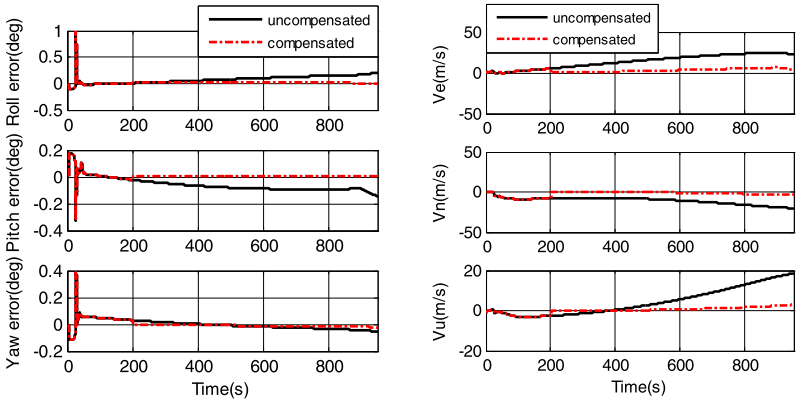


(a) Attitude error contrast curves (b) Velocity error contrast curves

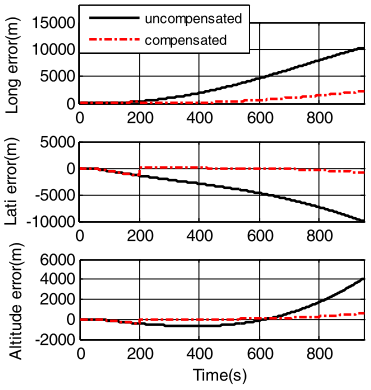


(c) Position error contrast curves

**Fig. 5.** Contrast results with the compensation of both IMU errors and the INS errors.

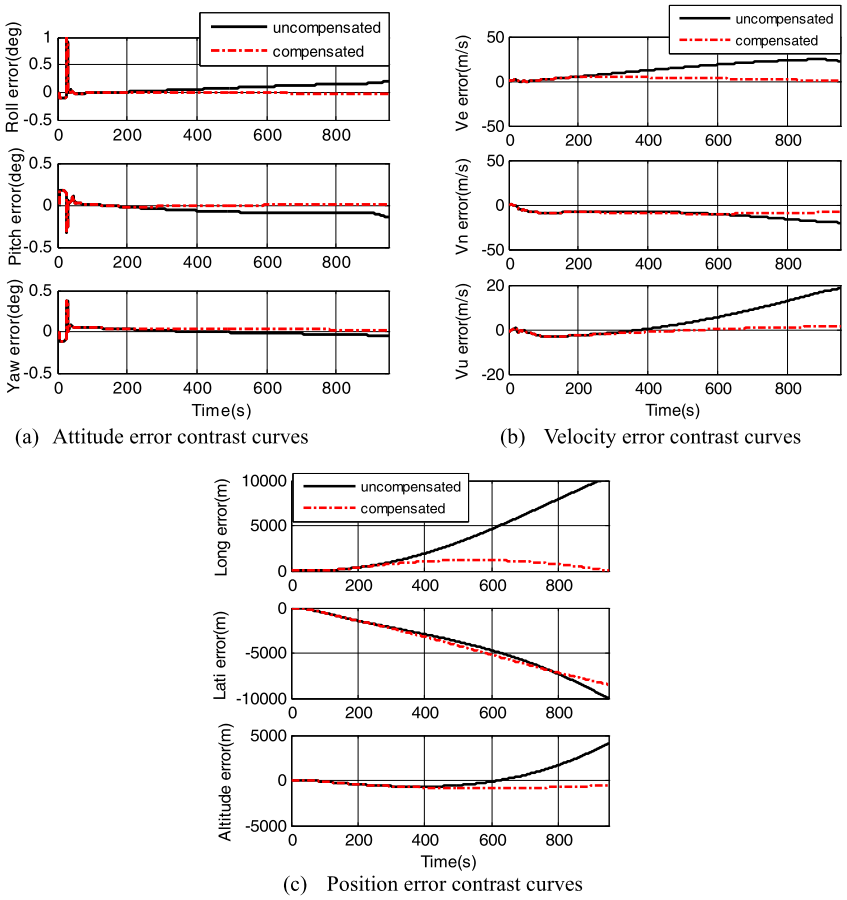


**Fig. 6.** Contrast results with the compensation of the IMU deterministic errors.

**Table 5**
RMS error contrast between the compensated and uncompensated INS.

| Error type | | Attitude error (units: arc second) | | | Velocity error (units: m/s) | | | Position error ($n$ mile/h) |
|---|---|---|---|---|---|---|---|---|
| | | Roll | Pitch | Yaw | East | North | Up | CEP |
| Uncompensated | | 389.16 | 291.86 | 90.98 | 17.96 | 12.23 | 8.78 | 15.89 |
| Compensated | first | 48.96 | 19.49 | 44.87 | 3.60 | 1.70 | 1.27 | 1.90 |
| | second | 62.62 | 34.00 | 80.54 | 3.41 | 9.38 | 1.20 | 12.32 |

when the vehicle was about to be in the cruise flight stage in Table 3. The start of the abscissa 0 s corresponds with the start of the designed trajectory in Table 3.

In order to reduce the accumulated errors of the INS navigation parameters, except the IMU deterministic errors, the IMU stochastic errors and the parameter errors of INS are also compensated; the compensate results are shown in Fig. 5.

In order to validate the calibration method for the IMU deterministic errors, only should the IMU deterministic errors be compensated and the results are shown in Fig. 6.

In both Fig. 5 and Fig. 6, the black solid lines represent the INS parameter errors without the compensation; the red dash dot lines represent the INS parameter errors with the compensation. Table 5 shows the RMS (Root Mean Square) errors of the compensated and uncompensated INS parameter errors.

In Table 5, the first group of the compensated results corresponds to the results shown in Fig. 5, i.e. the results with the compensation of the IMU errors and the INS parameter errors. The second group of the compensated results corresponds to the results with the compensation of the IMU deterministic errors.

From the contrast curves shown in Fig. 6 and Table 5, we can see that with only the compensation of the IMU deterministic errors, the diffuse trend of the INS is reduced; the INS parameter errors are reduced. With the calibration results of the IMU deterministic errors, the installation errors and the scale factor errors of the IMU are compensated and the parameter errors of the INS are reduced.

## 5. Conclusions

This paper presents a dynamic calibration research on the IMU deterministic errors of the INS for the hypersonic cruise vehicles. In this paper, an augmented IMU error model including the installation errors and the scale factor errors has been built; the INS parameter error equations that including the installation errors and scale factor errors of the IMU have been derived. Then, the improved Kalman Filter model has been composed and the dynamic calibration method for the IMU deterministic errors is proposed. The simulation results show that the dynamic calibration method can calibrate the installation errors and the scale factor errors effectively. The calibration results are used to compensate the IMU deterministic errors and the simulation results show that the precision of the compensated INS is improved.

## Acknowledgements

This work was partially supported by the National Natural Science Foundation of China (Grant Nos. 91016019, 61374115, 61210306075), the Aeronautic Science Foundation of China contract (Grant No. 2011ZC52044), the Priority Academic Program Development of Jiangsu Higher Education Institutions, the Funding for Outstanding Doctoral Dissertation in NUAA (Grant No. BCXJ10-05), the Fundamental Research Funds for the Central Universities, the peak of six personnel in Jiangsu Province, the Nanjing University of Aeronautics and Astronautics Special Research Funding, in part sponsored by Qing Lan Project of Jiangsu Province (Grant No. NP2012505), and the China Scholarship Council. The author would like to thank the anonymous reviewers for helpful comments and valuable remarks.

## References

[1] Catherine Bahm, Ethan Baumann, John Martin, David Bose, Roger E. Beck, Brian Strovers, The X-43A hyper-X Mach 7 flight 2 guidance, navigation and control overview and flight test, AIAA paper 2005-3275, 2005.
[2] Ethan Baumann, Catherine Bahm, Brian Strovers, Roger Beck, Michael Richard, The X-43A six degree of freedom Monte Carlo analysis, in: 46th AIAA Aerospace Sciences Meeting and Exhibit, January 2008.
[3] Serge M. Boldyrev, Volf Ya. Borovoya, Andrey Yu. Chinilov, Victor N. Gusev, et al., A thorough experimental investigation of shock/shock interferences in high Mach number flows, Aerosp. Sci. Technol. 5 (2001) 167–178.
[4] Luo Chao, Research on Calibration and Error Compensation for FOG SINS, Harbin Engineering University, 2006, pp. 9–24.
[5] Witold Ilewicz, Aleksander Nawrat, Direct method of IMU calibration, in: Advanced Technologies for Intelligent Systems of National Border Security, Stud. Comput. Intell. 440 (2013) 155–171.
[6] Dongkyu Lee, Sangchul Lee, Sanghyuk Park, Sangho Ko, Test and error parameter estimation for MEMS-based low cost IMU calibration, Int. J. Precis. Eng. Manuf. 12 (4) (2011) 597–603.
[7] Baiqi Liu, Jiancheng Fang, Novel field calibration through rotation in six-position for FOG-IMU, Opto-Electron. Eng. 35 (1) (2008) 60–65.
[8] John D. Schierman, David G. Ward, Jason R. Hull, Jeffrey F. Monaco, Adaptive guidance systems for hypersonic reusable launch vehicles, in: IEEE Aerosp. Conf. Proc., 2001, pp. 2657–2668.
[9] S.C. Shen, C.J. Chen, H.J. Huang, A new calibration method for MEMS inertial sensor module, in: International Workshop on Advanced Motion Control Conference, IEEE, 2010, pp. 106–111.
[10] Donald I. Soloway, Peter J. Ouzts, David H. Wolpert, et al., The role of guidance, navigation, and control, in: Hypersonic Vehicle Multidisciplinary Design and Optimization, 16th AIAA/DLR/DGLR International Space Planes and Hypersonic Systems and Technologies Conference, 2009-7329.
[11] Z.F. Syed, P. Aggarwal, C. Goodall, X. Niu, N. El-Sheimy, A new multi-position calibration method for MEMS inertial navigation systems, Meas. Sci. Technol. 18 (7) (2007) 1897–1907.
[12] D.H. Titterton, J.L. Weston, Strapdown Inertial Navigation Technology, Peter Peregrinus Ltd./IEE, London, 1997.
[13] Rong Wang, Jianye Liu, Zhi Xiong, Qinghua Zeng, Double-layer fusion algorithm for EGI-based system, Aircraft Eng. Aerosp. Technol. 85 (4) (2013) 258–266.
[14] Wei Wang, Zong-yu Liu, Rong-rong Xie, Quadratic extended Kalman filter approach for GPS/INS integration, Aerosp. Sci. Technol. 10 (2006) 709–713.
[15] Xinlong Wang, Fast alignment and calibration algorithms for inertial navigation system, Aerosp. Sci. Technol. 13 (2009) 204–209.
[16] Jinliang Zhang, Yongyuan Qin, Feng Wu, Technique for in-flight calibrating installation errors in multi-IMU redundancy system, in: International Conference on Information Technology and Software Engineering, 2012, pp. 99–108.
[17] Tao Zhang, Xiaosu Xu, A new method of seamless land navigation for GPS/INS integrated system, Measurement 45 (2012) 691–701.
[18] Xiong Zhi, Ji-hui Chen, Rong Wang, Jian-ye Liu, A new dynamic vector formed information sharing algorithm in federated filter, Aerosp. Sci. Technol. 29 (2013) 37–46.
[19] Guangtao Zhou, Jian Wang, Kai Li, Analysis of singular value under Kalman filtering for strapdown inertial system online calibration, in: Informatics in Control, Automation and Robotics, Lect. Notes Electr. Eng. 132 (2011) 779–784.